UPPSALA
UNIVERSITET

Digital Comprehensive Summaries of Uppsala Dissertations from the Faculty of Science and Technology 731

Ultrafast Coherent X-ray Diffractive Nanoimaging

FILIPE R. N. C. MAIA

ACTA
UNIVERSITATIS
UPSALIENSIS
UPPSALA
2010

ISSN 1651-6214
ISBN 978-91-554-7776-9
urn:nbn:se:uu:diva-121930

Dissertation presented at Uppsala University to be publicly examined in B41, BMC, Husargatan 3, Uppsala, Friday, May 14, 2010 at 13:15 for the degree of Doctor of Philosophy. The examination will be conducted in English.

Abstract
R. N. C. Maia, F. 2010. Ultrafast Coherent X-ray Diffractive Nanoimaging. Acta Universitatis Upsaliensis. *Digital Comprehensive Summaries of Uppsala Dissertations from the Faculty of Science and Technology* 731. 49 pp. Uppsala. ISBN 978-91-554-7776-9.

X-ray lasers are creating unprecedented research opportunities in physics,chemistry and biology. The peak brightness of these lasers exceeds presentsynchrotrons by 10^{10}, the coherence degeneracy parameters exceedsynchrotrons by 10^{9}, and the time resolution is 10^{5} times better. In theduration of a single flash, the beam focused to a micron-sized spot has the samepower density as all the sunlight hitting the Earth, focused to a millimetresquare. Ultrafast coherent X-ray diffractive imaging (CXDI) with X-ray lasers exploitsthese unique properties of X-ray lasers to obtain high-resolution structures fornon-crystalline biological (and other) objects. In such an experiment, thesample is quickly vaporised, but not before sufficient scattered light can berecorded. The continuous diffraction pattern can then be phased and thestructure of a more or less undamaged sample recovered% (speed of light vs. speed of a shock wave).This thesis presents results from the first ultrafast X-ray diffractive imagingexperiments with linear accelerator-driven free-electron lasers and fromoptically-driven table-top X-ray lasers. It also explores the possibility ofinvestigating phase transitions in crystals by X-ray lasers. An important problem with ultrafast CXDI of small samples such as single proteinmolecules is that the signal from a single measurement will be small, requiringsignal enhancement by averaging over multiple equivalent samples. We present anumerical investigation of the problems, including the case where samplemolecules are not exactly identical, and propose tentative solutions. A new software package (Hawk) has been developed for data processing and imagereconstruction. Hawk is the first publicly available software package in thisarea, and it is released as an open source software with the aspiration offostering the development of this field.

Keywords: XFEL, Phasing, Image Reconstruction, Single Particle Imaging, Ultrafast Diffraction, X-ray diffraction, Coherent Diffractive Imaging, CXDI

Filipe R. N. C. Maia, Department of ALM, Box 625, Uppsala University, SE-75126 Uppsala, SwedenMolecular biophysics, Box 596, Uppsala University, SE-75124 Uppsala, Sweden

ISSN 1651-6214
ISBN 978-91-554-7776-9
urn:nbn:se:uu:diva-122002 (http://urn.kb.se/resolve?urn=urn:nbn:se:uu:diva-122002)

to my grandparents...

List of Publications

This thesis is based on the following papers, which are referred to in the text by their Roman numerals.

I Chapman, H.N., Barty, A., Bogan, M.J., Boutet, S., Frank, M., Hau-Riege, S.P., Marchesini, S., Woods, B.W., Bajt, S., Benner, H., London, R.A., Plonjes, E., Kuhlmann, M., Treusch, R., Dusterer, S., Tschentscher, T., Schneider, J.R., Spiller, E., Moller, T., Bostedt, C., Hoener, M., Shapiro, D.A., Hodgson, K.O., Van der Spoel, D., Burmeister, F., Bergh, M., Caleman, C., Huldt, G., Seibert, M.M., Maia, F.R.N.C., Lee, R.W., Szoke, A., Timneanu, N., Hajdu J. (2006) Femtosecond diffractive imaging with a soft-X-ray free-electron laser. *Nature Physics*, 2(12):839-843

II van der Spoel, D., Maia, F.R.N.C., Caleman, C. (2008), Structural studies of melting on the picosecond time scale. *Physical Chemistry Chemical Physics*,10(42):6344-6349

III Ravasio, A., Gauthier, D., Maia, F.R.N.C., Billon, M., Caumes, J.P., Garzella, D., Geleoc, M., Gobert, O., Hergott, J.F., Pena, A.M., Perez, H., Carre, B., Bourhis, E., Gierak, J., Madouri, A., Mailly, D., Schiedt, B., Fajardo, M., Gautier, J., Zeitoun, P., Bucksbaum, P.H., Hajdu, J., Merdji, H. (2009) Single-Shot Diffractive Imaging with a Table-Top Femtosecond Soft X-Ray Laser-Harmonics Source. *Physical Review Letters*, 103:028104

IV Maia, F.R.N.C., Ekeberg, T., Tîmneanu, N., van der Spoel, D., Hajdu, J. (2009) Structural variability and the incoherent addition of scattered intensities in single-particle diffraction. *Physical Review E*, 80:031905

V Maia, F.R.N.C., Ekeberg, T., van der Spoel, D., Hajdu, J. (2010) Hawk: the image reconstruction package for coherent X-ray diffractive imaging. *Submitted for publication*

Supporting Publications

VI Bergh, M., Huldt, G., Tîmneanu, N., Maia, F.R.N.C., Hajdu, J. (2008) Feasibility of imaging living cells at subnanometer resolutions by ultrafast X-ray diffraction. *Quarterly Reviews of Biophysics*, 41(3-4):181-204

VII Bogan, M.J., Benner, W.H., Boutet, S., Rohner, U., Frank, M., Barty, A., Seibert, M.M., Maia, F., Marchesini, S., Bajt, S., Woods, B., Riot, V., Hau-Riege, S.P., Svenda, M., Marklund, E., Spiller, E., Hajdu, J., Chapman, H.N. (2008) Single particle X-ray diffractive imaging. *Nano Letters*, 8(1):310-316

Contents

Abbreviations

CXDI	Coherent X-ray Diffraction Imaging
CPU	Central Processing Unit
CUDA	Compute Unified Device Architecture
DESY	Deutsches Elektronen Synchrotron
DNA	Deoxyribonucleic acid
FEL	Free Electron Laser
FFT	Fast Fourier Transform
FLASH	Free Electron Laser in Hamburg
fs	femtosecond
GPU	Graphics Processing Unit
HHG	High harmonic generation
HIO	Hybrid-Input Output
LCLS	Linac Coherent Light Source
PRTF	Phase Retreival Transfer Function
RAAR	Relaxed Averaging Alternating Reflection
RNA	Ribonucleic acid
SASE	Self Amplified Spontaneous Emission
SCSS	Spring-8 Compact Sase Source
SLAC	Stanford Linear Accelerator Center
VUV	Vacuum Ultra Violet
XFEL	European X-ray Free Electron Laser

1. Introduction

"The history of the living world can be summarized as the elaboration of ever more perfect eyes within a cosmos in which there is always something more to be seen" wrote Pierre Teilhard de Chardin in *The Phenomenon of Man* (1955). In the early sixteen hundreds, members of the Accademia dei Lincei in Rome decided to split the task of exploring the world around us: Gallileo was to study things big while Stelluti and Cesi were to explore the microscopic world. 300 yeares later, a fundamental barrier was taken down through the invention of X-ray crystallography, which made it possible to observe structures much smaller than the wavelength of visible light.

X-ray crystallography is one of the most successful techniques ever developed for the study of structures in atomic details. It has had a huge impact on biology, e.g. through the discovery of the structure of DNA, RNA, proteins and their complexes. Every year thousands of new structures are solved and deposited in the Protein Data Bank. Cryo electron microscopy also shows great promise with current structures frequently achieving resolutions below 10 Å, but still not enough for atomic resolution.

However, X-ray crystallography, as the name suggests, is limited to systems that can be crystallized. Many, if not most, systems of biological interest are very difficult, or impossible to crystallize. Probably the most striking example is that of a simple cell, but there are many others such as organelles, glycoproteins and many membrane proteins. Alternative approaches have to be employed to image these samples.

Ultrafast Coherent X-ray Diffractive Imaging (CXDI) is a relatively new technique, which uses a coherent, short and extremely bright pulse of X-rays to capture a diffraction image of the sample which is then phased to reveal the sample structure. CXDI has the potential to allow three dimensional imaging of nonperiodic reproducible biological samples up to atomic resolution and two dimensional imaging of non reproducible samples up to very high resolution, without the need of modifying the sample.

CXDI does not benefict from the amplification effect of a crystal as X-ray crystallography does. But on the other hand it is possible to sample the diffraction pattern continuously which makes the phasing problem much simpler. To be able to achieve high resolution using CXDI, very short and intense pulses are necessary otherwise the radiation damage that develops during the exposure limits the maximum resolution. For example, the highest resolution

possible for biological samples using current synchrotron based x-ray microscopes is around 20nm, limited by radiation damage [21].

The recent development of X-ray free-electron lasers (FELs) gives a perfect instrument to realize the full potential of CXDI. X-ray FELs can produce extremely intense X-ray pulses, a billion times more brilliant than third generation synchrotron sources. X-ray FEL pulses are also extremely short, on the order of only a few femtoseconds. FLASH, in Hamburg, Germany, was the first soft X-ray free electron laser in the world, and is based on the Self Amplified Spontaneous Emission (SASE) principle. It started operations in the summer of 2005 at a wavelength of 32nm and a peak power on the order of gigawatts and pulse length as short as 10fs. It has gone through several updates reaching the wavelength of 6.5nm. FLASH is a test facility for the European X-ray Free Electron Laser (XFEL), and it has produced many important results in the CXDI field [9, 11]. In April 2009 the Linac Coherent Light Source (LCLS) became the first hard X-ray free electron laser in the world producing light with a wavelength of 1.5 Å. The Spring-8 Compact SASE Source (SCSS) in Japan will soon be ready and the XFEL will follow in a few years.

During the last few years there has also been a rapid development of table-top high harmonic generation (HHG) sources. These have the potential to compete one day with free electron lasers and they are much more affordable for individual labs. Nowadays there are HHG sources with very good coherence properties capable of producing extremely short pulses, under 1fs, at soft X-ray wavelengths and more than 10^{11} photons per pulse [35]. This is still a few orders of magnitude below what is possible using accelerator-based FELs but progress is fast, and those sources might become very important tools in the near future.

The availability in the near future of several hard X-ray FELs combined with the increasing development of CXDI experimental techniques and data processing algorithms have the potential to transform Ultrafast Coherent X-ray Diffractive Imaging from a niche of unconventional techniques into a mainstream structural biology tool that complements X-ray crystallography or electron microscopy.

The aims of this thesis are: to present recent experimental results in Ultrafast Coherent X-ray Diffractive Imaging using both free electron lasers and optically-driven table-top X-ray laser, to theoretically investigate the problem of sample heterogeneity for reproducible samples and to propose new experiments made possible with these new sources.

2. X-ray Lasers

Since the discovery of X-rays by Wilhelm Röntgen in 1895 X-ray sources have continuously improved, often leading to significant new science. The increase in brilliance since the first rotating anodes used for crystallography has been spectacular, bridging many orders of magnitude. The development of dedicated synchrotron light sources in the beggining of the 80s contributed to an explosion of protein structures solved by crystallography. A further boost came with the introduction of wigglers, undulators and the increase in brightness from third generation sources, which employ them.

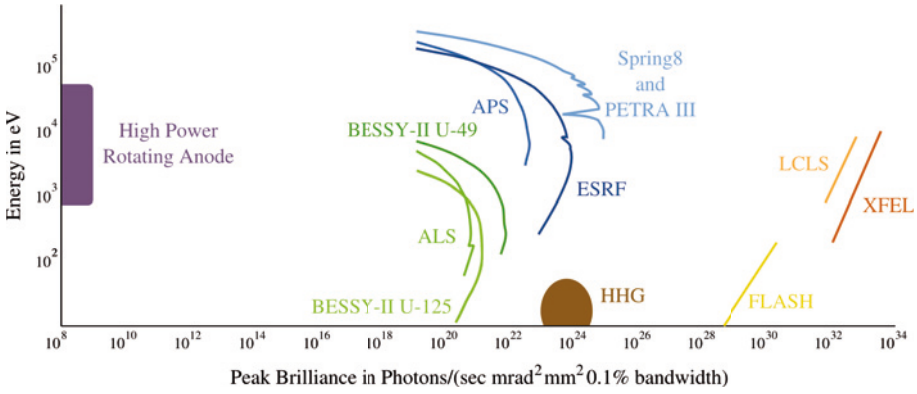

Figure 2.1: Peak brilliance of several X-ray sources. Adapted from [1, 29]

Yet the first dedicated synchrotron source (the SRS Daresbury) which began user operation in 1981, produced just about 40 times higher beam intensities on the sample than a laboratory X-ray generator. The synchrotron beam had better coherence parameters, and it was tunable, but overall, the improvement was evolutionary. X-ray lasers are different. The peak brightness of these lasers exceeds present synchrotrons by 10^{10}, the coherence degeneracy parameters exceed synchrotrons by 10^9, and the time resolution is 10^5 times better. These developments are extraordinary. The results will impact on a broad range of disciplines, and guide technology and facility development in the future.

2.1 Linear Accelerator-Driven Free-Electron Lasers

A free-electron laser (FEL) is a parametric amplifier, which operates by transferring energy to the output signal from an oscillator. An electron bunch is accelerated to relativistic energies, and sent through a periodic magnetic structure (undulator) where transverse oscillations and interference produce synchrotron radiation enhanced at specific wavelengths. The intensity of this radiation scales with the number of electrons in the bunch. Photons co-propagate with the relativistic electrons and, if the undulator is long enough, induce an energy modulation, leading to a periodic density modulation in the electron cloud. The resulting microbunches behave like giant charged particles, and emit photons proportional to the square of their total charge in the undulator. At wavelengths longer than the bunch length, this radiation is coherent.

Optically driven table-top X-ray lasers use an intense optical laser pulse to create coherent X-ray pulses in a plasma. The interaction of intense optical fields with material at intensities of 10^{18} W/cm^2 and above is governed by the electron relativistic behaviour, creating the domain of relativistic optics. Electrons accelerated in such photon fields can be used in ultra-brilliant X-ray sources, e.g. by laser-assisted synchrotron radiation, linear and nonlinear Compton scattering, betatron radiation or free-electron-laser mechanisms. Currently these sources are not quite as powerful as FELs but progress is fast, and table-top X-ray lasers may catch up with large linac-based FELs.

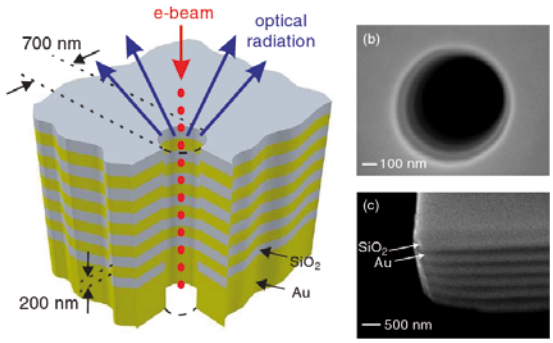

Figure 2.2: (a) Schematic cut-away section of a light well, which comprises a nanohole through a stack of alternating metal and dielectric layers, into which an electron beam is launched. Light is generated as electrons travel down the well and encounter a periodic material environment. (b) Scanning electron microscope image of a light well fabricated in a gold- silica multilayer. (c) The alternating metal-dielectric layer structure as seen at an exposed corner of the sample. [2]

X-ray lasers are bound to get smaller, more efficient and more affordable. A recent paper describes a *free-electron laser on a chip* (see Fig. 2.2). The tiny FEL utilises the Smith-Purcell effect [39], which is related to Cherenkov radiation.

There are signs that indicate that a major scientific explosion is taking shape.

2.1.1 The SASE process

The SASE process, central to all existing X-ray free electron lasers, is a process in which the electrons are organized into micro bunches separated by the distance of a wavelength, as they go through the undulator (see Fig. 2.3). This happens because, as in a normal synchrotron, when the electrons go through the undulator they emit radiation due to the acceleration imposed by the magnetic field. If the undulator is sufficiently long, this radiation starts to produce a measurable effect in the distribution of the electrons making them accumulate in micro bunches separated by exactly one wavelength. This is a self reinforcing process as the more the electrons bunch together the stronger the field they produce as they will radiate coherently. This process continues until almost all the electrons are in these micro-bunches, at which point saturation is reached. Under these conditions the microbunches behave like giant single particles and emit light proportional to the square of their total charge.

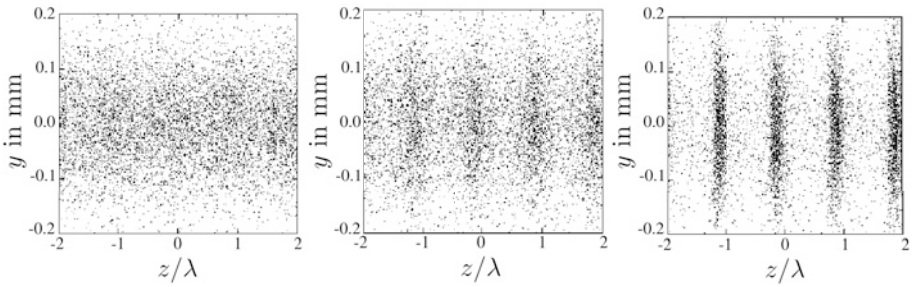

Figure 2.3: Simulation of micro-bunching during the SASE process where the electron density is represented by the density of dots. The snapshots from the left to the right represent the electron structure along the undulator, with the left side representing the beginning and the right side the end of the undulator. [29]

The radiation produced by electrons distributed in this manner is much more intense than if the electrons were uniformly distributed throughout the undulator because with microbunching the distance between most of the electrons is always a multiple of the wavelength, and so the radiated electric fields will be in phase. In other words, the electrons radiate coherently and the resulting intensity scales with the square of the number of electrons which is why the difference in peak brilliance is so large.

2.1.2 Current X-ray FEL Facilities

X-ray FEL are developing at a very fast pace. The first hard X-ray FEL, the LCLS, began user operations in October 2009. There are several X-ray FELs

being built such as the European XFEL in Germany and SCSS in Japan, as well as several soft X-ray sources such as FERMI and SPARX in Italy. The SwissFEL in Switzerland is also in planning stages. The different characteristics of FEL radiation compared to a third generation synchrotron mean that while they are often called fourth generation sources they will not replace synchrotrons in any meaningful sense. X-ray lasers should be considered a class of their own better suited for other kinds of experiments than those possible at synchrotrons.

2.2 Optically-Driven Table-Top X-ray Lasers

The first high harmonic generation (HHG) sources were created about two decades ago and since then their power has been increasing as the power of all lasers usually increases. They provide a relatively cheap and tunable source of very short (a few fs) and intense pulses (more than 10^{10} photons per pulse).

HHG works by shining a very intense optical laser into a gas. When the field of the optical laser is sufficiently strong electrons in the gas will be ionized by field ionization, and as the field progresses they will be accelerated back towards the ion and finally recombine, generating in the process short wavelength radiation (see Fig. 2.4).

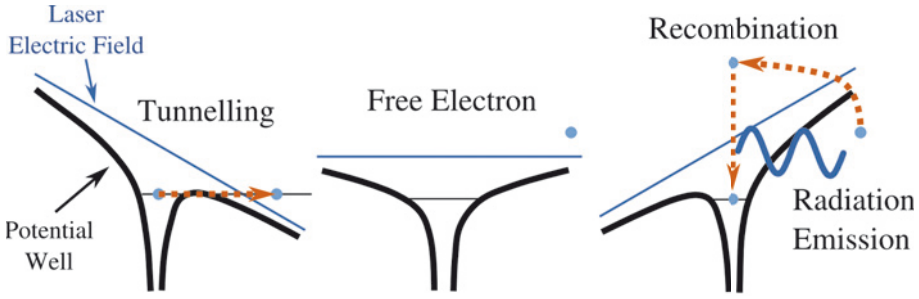

Figure 2.4: High harmonic generation process in an atom illuminated by an intense optical laser. The field is strong enough to distort the atomic potential well and allowing the electron to tunnel out. When the field reverses the electron is accelerated back towards the ion. Radiative recombination generates high energy radiation. [12, 23]

3. An Introduction to Fourier Transforms

Fourier transforms are used extensively in the subject of diffraction and imaging, so in this chapter we present a basic introduction, describing the Fourier transform and its most commonly used properties. These properties will be fundamental for a description of scattering and for the explanation of image reconstruction algorithms.

3.1 Continuous Fourier Transform

We will start by defining the continuous forward Fourier transform, following crystallographic tradition, as,

$$\hat{f}(q) = \mathcal{F}f = \int_{-\infty}^{\infty} f(x)\exp(2\pi i q\cdot x)\,dx \tag{3.1}$$

and the inverse transform as

$$f(x) = \mathcal{F}^{-1}\hat{f} = \int_{-\infty}^{\infty} \hat{f}(q)\exp(-2\pi i q\cdot x)\,dq. \tag{3.2}$$

The following properties of the Fourier transform will be important for the rest of the thesis:

1. The Fourier transform is a linear transformation. For any two complex numbers a and b

$$\mathcal{F}\{af(x)+bg(x)\} = a\mathcal{F}f(x)+b\mathcal{F}g(x) \tag{3.3}$$

2. "Stretching" a function "squeezes" its Fourier transform,

$$\mathcal{F}\{f(ax)\} = \frac{1}{|a|}\hat{f}(\frac{x}{a}) \tag{3.4}$$

where a is a real number different from zero. This is known as the scaling property or theorem.

3. The Fourier transform of a real function $f(x)$ is a hermitian function,

$$\hat{f}(q) = \overline{\hat{f}(-q)} \tag{3.5}$$

where $\overline{\hat{f}(-q)}$ represents the complex conjugate of $\hat{f}(-q)$.

4. The Fourier transform of an hermitian function $f(x)$ is a real function,

$$Im\left[\hat{f}(q)\right] = 0 \tag{3.6}$$

where $Im\left[\hat{f}(q)\right]$ represents the imaginary part of $\hat{f}(q)$.

5. The Fourier transform of a function translated by an amount Δx is related to the transform of the original function by a factor of $\exp(2\pi i \Delta x q)$,

$$\mathcal{F}f(x+\Delta x) = \exp(2\pi i \Delta x q)\mathcal{F}f(x) \tag{3.7}$$

6. The integral of the square of the absolute value of a function and it's Fourier transform are identical

$$\int |\hat{f}(q)|^2 dq = \int |f(x)|^2 dx. \tag{3.8}$$

This is usually known as Parseval's theorem or Rayleigh's energy theorem.

7. The convolution of any two functions is equal to the inverse Fourier transform of the product of the forward Fourier transform of those two functions,

$$\begin{aligned} f(x) * g(x) &= \int f(\tau) g(x-\tau)\, d\tau \\ &= \mathcal{F}^{-1}\left\{\mathcal{F}f(x) \times \mathcal{F}g(x)\right\} \end{aligned} \tag{3.9}$$

where $f(x) * g(x)$ denotes the convolution of $f(x)$ with $g(x)$. This property is known as the convolution theorem.

8. The cross-correlation of any two functions is equal to the inverse Fourier transform of the product of the forward Fourier transform of one function with the complex conjugate of the forward Fourier transform of the other function,

$$\begin{aligned} f(x) \star g(x) &= \int f(\tau) g(x+\tau)\, d\tau \\ &= \mathcal{F}^{-1}\left\{\mathcal{F}f(x) \times \overline{\mathcal{F}g(x)}\right\} \end{aligned} \tag{3.10}$$

where $f(x) \star g(x)$ denotes the cross-correlation of $f(x)$ with $g(x)$.

9. Finally the correlation of a function with itself, also known as autocorrelation is equal to the inverse Fourier transform of the absolute value squared

of the forward Fourier transform of that function,

$$\begin{aligned} f(x) \star f(x) &= \mathcal{F}^{-1}\left\{\mathcal{F}f(x) \times \overline{\mathcal{F}f(x)}\right\} \\ &= \mathcal{F}^{-1}\left\{|\mathcal{F}f(x)|^2\right\} \end{aligned} \tag{3.11}$$

3.2 Discrete Fourier Transform

In practice we will be dealing with signals which are not continuous, but discrete, as most signal recording is done digitally nowadays and to be able to perform numerical computations with any input we first need to digitize it. Fortunately there is a discrete analogue of the Fourier transform called the discrete Fourier transform (DFT). The one dimensional discrete Fourier transform of a vector $\mathbf{x}$ of length N is defined by

$$\hat{\mathbf{x}}_k = \mathcal{F}\{\mathbf{x}\}_k = \frac{1}{\sqrt{N}} \sum_{n=0}^{N} \mathbf{x}_n \exp\left(2\pi i k \frac{n}{N}\right), \tag{3.12}$$

and the inverse pair as

$$\mathbf{x}_n = \mathcal{F}^{-1}\{\mathbf{x}\}_n = \frac{1}{\sqrt{M}} \sum_{k=0}^{M} \hat{\mathbf{x}}_k \exp\left(-2\pi i n \frac{k}{M}\right). \tag{3.13}$$

Throughout this thesis we will commit a slight abuse of notation and use $\mathcal{F}$ to symbolize both the continuous Fourier transform, when the operand is a function, and the discrete Fourier transform, when the operand is a vector.

The DFT has properties analogous to most properties of its continuous counterpart, in particular it is a distance preserving transform, that is, the distance between two vectors is the same before and after transformation

$$|\mathcal{F}(x) - \mathcal{F}(y)| = |(x - y)| \tag{3.14}$$

which follows from both the linearity of the transform and Parseval's theorem. It also fulfills the convolution theorem if we define the discrete convolution as

$$(\mathbf{a} * \mathbf{b})_n = \sum_{m=0}^{N-1} \mathbf{a}_m \mathbf{b}_{n-m \bmod N}. \tag{3.15}$$

Notice the modulus N in the index of b. This detail will lead to important consequences.

3.3 Sampling and oversampling

An arbitrary band-limited signal $f(x)$ with bandwidth $2B$, meaning a signal which has $\hat{f}(x) = 0$ for every $|x| > B$, can be perfectly reconstructed from the same signal sampled in steps of length smaller or equal to $1/2B$ [38]. $2B$ is known as the *Nyquist rate*. This derives from the fact that the continuous Fourier transform of $f(x)$ can be exactly reconstructed from equidistant samples separated by a step of length $s < 1/2B$,

$$rect_B(q) = \begin{cases} 1 & \text{if } |q| \leq B, \\ 0 & \text{if } q > B. \end{cases} \tag{3.16}$$

$$\text{Ш}_s(x) = \sum_{i=-\infty}^{\infty} \delta(x - is) \tag{3.17}$$

$$\hat{f}(q) = \mathcal{F}\{\text{Ш}_s(x) f(x)\} rect_B(q) \tag{3.18}$$

where $\delta(x)$ represents the Dirac delta function.

As figure 3.1 shows, sampling a signal causes its spectrum to be replicated in Fourier space. The distance between the replicas is proportional to the sampling frequency due to the scaling property of the Fourier transform. If the sampling frequency is below the Nyquist rate the spectra will overlap and a perfect reconstruction is no longer possible. This phenomenon is known as aliasing (see Fig. 3.2) and is related to eq. 3.15. We call such a signal *undersampled*. If on the other hand the sampling frequency is higher than the Nyquist rate, we call it *oversampled* and we define the *oversampling ratio*, σ, as the ratio between the sampling frequency and the Nyquist rate or, equivalently, the fraction between the center of two replicas of the spectrum in Fourier space and the region for which the spectrum is different from zero, as illustrated in figure 3.3.

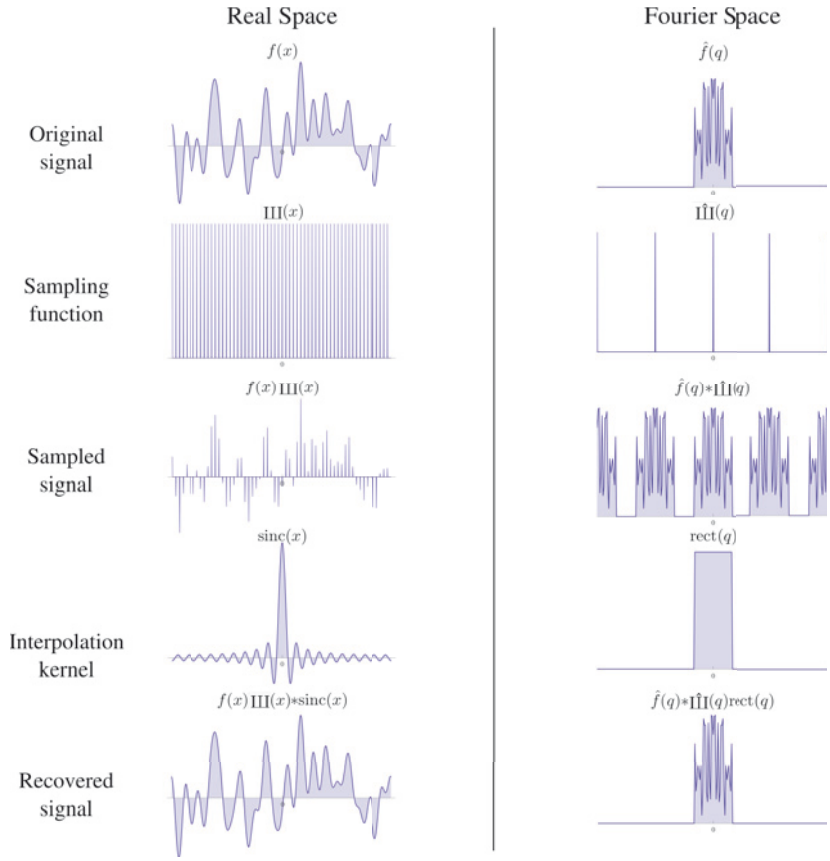

Figure 3.1: Reconstruction of a band-limited signal from discrete samples taken at a frequency higher than the Nyquist rate. The signal $f(x)$ is multiplied with the sampling function $\mathrm{III}(x)$ corresponding to sampling of the signal by a pixel detector. This corresponds to replicating the spectrum of the signal in Fourier space. Notice that there is no overlap of the replicated spectra of the sampled signal in Fourier space (on the right). It is then possible to recover the original signal by selecting it with an appropriate rectangular window function $\mathrm{rect}(q)$. In real space this corresponds to a convolution with the corresponding sinc function $\mathrm{sinc}(x)$.

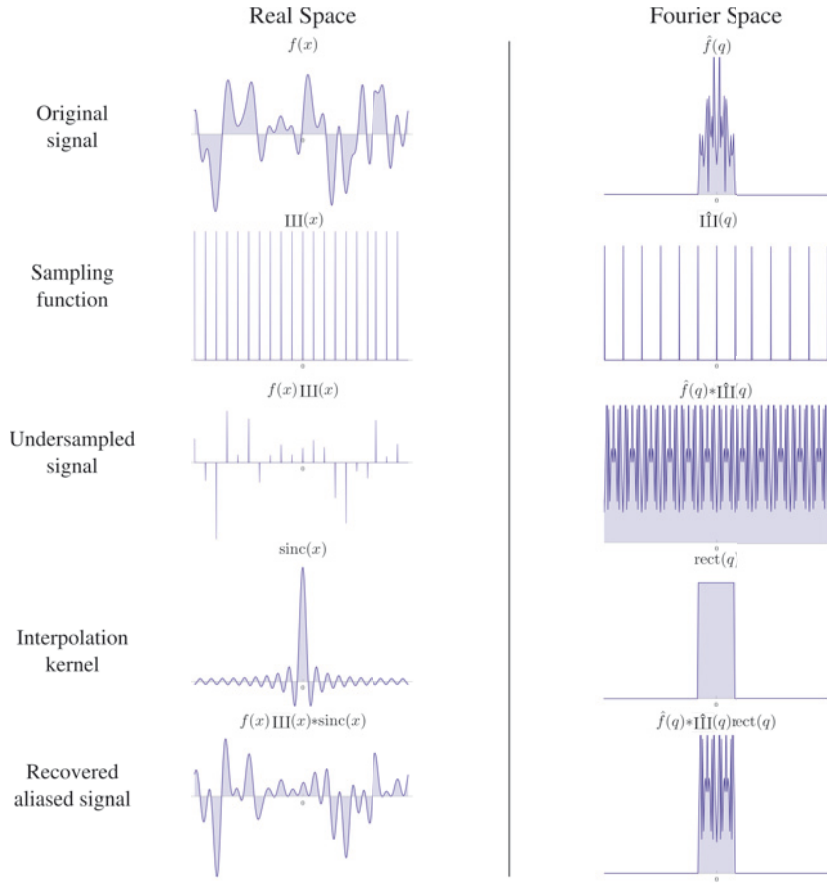

Figure 3.2: Incomplete recovery of an undersampled band-limited signal leading to aliasing. The process is analogous to 3.1 but with a sampling frequency below the Nyquist rate. The replicated spectra of the undersampled signal overlap with each other in Fourier space, and a perfect reconstruction is no longer possible.

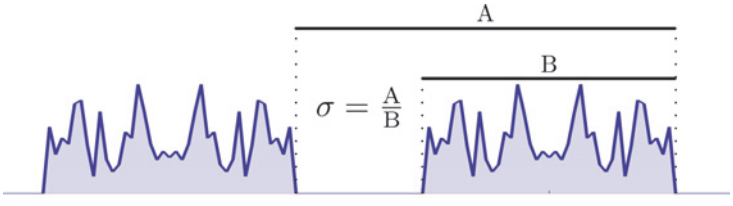

Figure 3.3: The oversampling ratio, denoted by σ, is the ratio between the size of the Fourier space and the region over which the signal is different than zero.

4. Theory of X-ray Diffraction by Matter

This chapter gives an overview of the most important tools necessary to understand X-ray diffraction and provides a simple framework for analysing most CXDI experiments based on the first-order Born approximation, also known as "kinematical" or "single-scattering" approximation. This will be of fundamental importance when we later try to reconstruct the object that gave rise to a certain diffraction pattern, as it is obviously impossible to do this if we cannot predict the diffraction pattern that a given object produces.

4.1 Scattering by a free electron

According to classical electromagnetic theory the electric field associated with a plane monochromatic wave of amplitude E_0, frequency ν, propagating along the z axis (Fig. 4.1a), is given by

$$E_i(z,t) = E_0 \exp(2\pi i \nu (t - z/c)) . \tag{4.1}$$

When such a wave travels through an electron of charge e and mass m located at the origin of a coordinate system, that electron will oscillate in the direction of the incident electric vector driven by

$$a(t) = \frac{eE_i(0,t)}{m} \tag{4.2}$$

with a frequency equal to the incoming wave. This in turn will make it radiate an electric field E_s, like any accelerating charge. It follows from Maxwell's equations that the electric field generated by an accelerating electron measured at $\mathbf{r}$ is given by

$$E_s(\mathbf{r},t) = \frac{ea_\perp(t - |\mathbf{r}|/c)}{4\pi\varepsilon_0 c^2 r} \tag{4.3}$$

where ε_0 is the permittivity of free space and $a_\perp$ is the acceleration projected on a plane normal to $\mathbf{r}$, also called the transverse component of the acceleration (Fig. 4.1b) [3]. Finally combining equations 4.1, 4.2 and 4.3 we get that

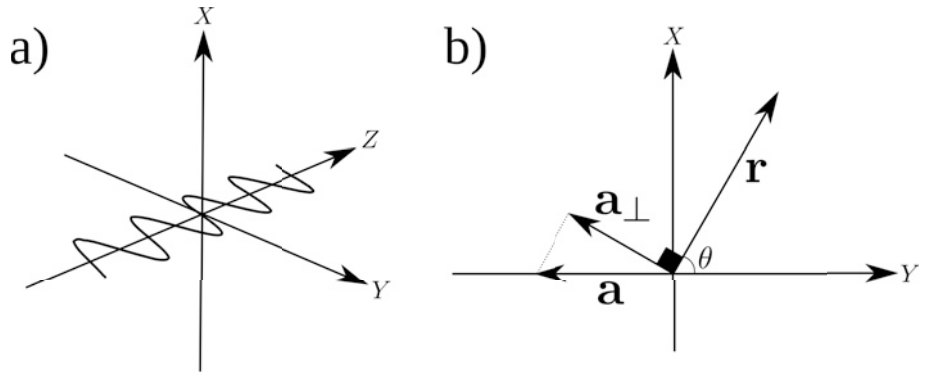

Figure 4.1: **a)** Monochromatic planar wave linearly polarized along the y axis propagating in the positive z direction. **b)** Transverse component of the acceleration sustained by the electron as observed from the position $\mathbf{r}$. θ is the angle between the polarization axis and the projection of $\mathbf{r}$ on a plane normal to the propagation direction.

the instantaneous scattered field by a free electron is

$$a_{\perp}(t) = |\mathbf{a}(t)| \sin\theta \tag{4.4}$$

$$E_s(\mathbf{r},t) = \frac{e^2 E_0 \sin\theta}{4\pi\varepsilon_0 mc^2 r} \exp(2\pi i\nu(t-|\mathbf{r}|/c)). \tag{4.5}$$

The classical electron radius is defined as

$$r_e = \frac{e^2}{4\pi\varepsilon_0 mc^2} \tag{4.6}$$

which can be used to simplify the electric field expression to

$$E_s(\mathbf{r},t) = \frac{r_e E_0 \sin\theta}{r} \exp(2\pi i\nu(t-|\mathbf{r}|/c)). \tag{4.7}$$

The time averaged scattered power per unit area normal to $\mathbf{r}$, also known as intensity, can then be obtained from the average length of the Poynting vector,

$$I(\mathbf{r}) = \frac{|E_{max}(\mathbf{r})|^2}{2\varepsilon_0 c}. \tag{4.8}$$

where E_{max} denotes the maximum value of the electric field. The time averaged power per unit area normal to $\mathbf{r}$ scattered by an electron is then

$$I(\mathbf{r}) = \frac{r_e^2 E_0^2 \sin^2\theta}{2\varepsilon_0 c r^2}, \tag{4.9}$$

The total scattered intensity by a free electron as a fraction of the incoming intensity, can now be calculated by integrating equation 4.9 over a spherical

shell of radius 1 around the electron,

$$I_0 = \frac{E_0^2}{2\varepsilon_0 c} \tag{4.10}$$

$$I_s = \int_0^{2\pi}\int_0^{\pi} \frac{r_e^2 E_0^2 \sin^2\theta}{2\varepsilon_0 c} \sin\theta d\theta d\phi = \frac{8\pi}{3}\frac{r_e^2 E_0^2}{2\varepsilon_0 c} \tag{4.11}$$

$$\sigma_T = \frac{I_s}{I_0} = \frac{8\pi}{3} r_e^2 \tag{4.12}$$

where I_0 represent the incoming intensity, I_s the scattered intensity and σ_T the ratio between the two, also known as the *scattering cross-section* for a free electron, also known as the Thomson cross-section after the British physicist J.J. Thomson who first derived it in the beginning of the 20th century. Elastic scattering by a free charged particle is also known as *Thomson scattering*.

4.2 Scattering by two electrons

If instead of just one electron we have a system composed of two or more electrons a new phenomenon is observed, *interference* between the waves scattered by the different electrons. We will start by looking at the most simple system where this occurs, one with just two electrons. We will keep the electron from the previous section at the origin and add a new electron at the position $\mathbf{r}$. When the system is illuminated by an electric field of amplitude E_0 traveling along $\mathbf{s}_0$, both electrons will scatter as described in Eq. 4.7. The amplitude of the scattered field from each electron is the same but the phase depends on the relative position of the two electrons (Fig. 4.2).

For an observer located at $\mathbf{d}$ in the direction of $\mathbf{s}$, at a distance much greater than the distance between the electrons the observed total electric field is the sum of the fields scattered by each of the electrons, which can be approximated by,

$$\Delta l = \Delta l_1 + \Delta l_2 = \mathbf{r}\cdot(\mathbf{s}_0 - \mathbf{s}) \tag{4.13}$$

$$E(\mathbf{d}) = E_s(\mathbf{d}) + E_s(\mathbf{d})\exp(\frac{2\pi i \Delta l}{\lambda}) \tag{4.14}$$

where $\mathbf{s}_0$ and $\mathbf{s}$ are unit vectors, Δl is the total path difference, E_s the electric field scattered by an isolated electron, λ the wavelength of the incoming field and E the total observed field. This approximation assumes that $|\mathbf{d}| - |\mathbf{d}-\mathbf{a}| << \lambda$, or put in another way $|\mathbf{r}|^2/(|\mathbf{d}|\lambda) \ll 1$. This approximation is known as the *Fraunhofer approximation* and the conditions under which they are valid are known as the far field regime. “Fraunhofer diffraction” is a term used to describe diffraction in this regime. Also implicit in this calculation is the assumption that the scattered field from one electron produces a

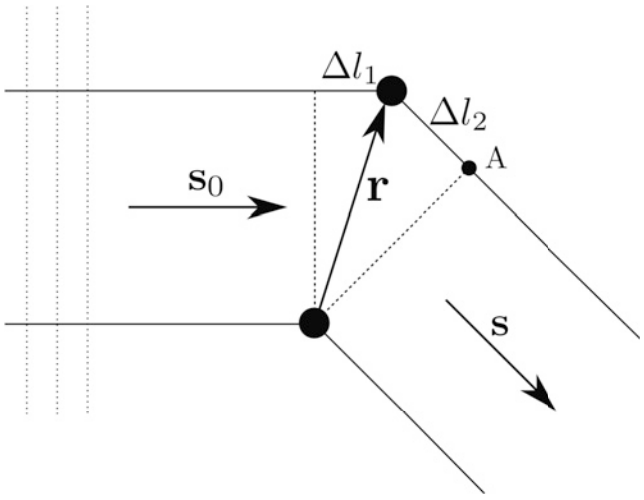

Figure 4.2: Monochromatic planar wave propagating along $\mathbf{s}_0$, shines on two electrons separated by $\mathbf{r}$. The observed scattered electric field on the direction $\mathbf{s}$ at a distance $|\mathbf{d}|$ much larger than $|\mathbf{r}|$ is the sum of two identical fields separated by a phase difference dependent on the path difference $\Delta l_1 + \Delta l_2$ [37].

negligible influence on the scattered field of the other electron, that is, multiple scattering can be ignored. This approximation is known as the *first-order Born approximation*. It is important to notice that the relative phase between the two electrons does not depend on the choice of origin and so the observed intensity is independent of the choice of origin, as it must obviously be.

4.3 Scattering by an arbitrary electron cloud

The two electron framework presented in the previous section can be easily extended to N electrons by noticing that the electrons scatter independently of each other. So the scattering of N electrons measured at a point $\mathbf{d}$ is given by

$$E(\mathbf{d}) = E_s(\mathbf{d}) \sum_{n=0}^{N} \exp\left(\frac{2\pi i \mathbf{r}_n \cdot (\mathbf{s}_0 - \mathbf{s})}{\lambda}\right). \tag{4.15}$$

The vector $\mathbf{S} = \frac{\mathbf{s}_0 - \mathbf{s}}{\lambda}$ is known in crystallography as the *scattering vector* and the surface drawn by the tip of the scattering vector while $\mathbf{s}$ is rotated around a sphere is known as the *Ewald sphere*.

The continuous case is now easily derived by replacing individual electrons by an electron density ρ. The scattering from an electron density cloud is then

described by

$$E(\mathbf{d}) = E_s(\mathbf{d}) \int_{\mathbf{r}} \rho(\mathbf{r}) \exp(2\pi i \mathbf{r} \cdot \mathbf{S})\, d\mathbf{r}. \tag{4.16}$$

We can now introduce the *structure factor*, defined as the ratio between the scattered field by the system and the scattered field by a single electron,

$$F(\mathbf{d}) = \frac{E(\mathbf{d})}{E_s(\mathbf{d})} = F\left(\frac{\mathbf{d}}{|\mathbf{d}|}\right) \tag{4.17}$$

The structure factor is a more useful quantity than the electric field as it does not depend on the distance to the detector, only on the direction of the observer and the structure of the system. For an arbitrary electron cloud the structure factor as a function of the scattering vector is given by,

$$F(\mathbf{S}) = \int_{\mathbf{r}} \rho(\mathbf{r}) \exp(2\pi i \mathbf{r} \cdot \mathbf{S})\, d\mathbf{r}, \tag{4.18}$$

which is simply the three dimensional Fourier transform of $\rho(\mathbf{r})$ evaluated at $\mathbf{S}$. It is for this reason that Fourier transforms are such a useful tool when studying diffraction, and why they were introduced in the previous chapter.

This formalism was used for the diffraction calculation in **paper II**.

4.4 Coherence

Throughout the previous sections we have assumed that the incoming wave was perfectly coherent, both temporaly and spatially (see Fig. 4.3). Temporal coherence is related to the bandwidth of the wave: the larger the bandwidth the worse is the coherence. We have assumed monochromatic waves i.e. perfect temporal coherence. Spatial coherence is a measure of how stable is the phase relation between two points as a function of time. More accurately it is the cross-correlation of the field at two locations over time [3].

Coherence is important for diffraction experiments [20, 43] because if, for example, the spatial coherence of the beam is low, the instantaneous diffraction pattern of our system will change rapidly during the exposure, but the integrated pattern will show very few signs of interference between different parts of the system and so hide its structure. We can see this by comparing the diffraction pattern obtrain from the field in Eq. 4.14, to the one generated by replacing $\Delta l/\lambda$ by a random term X between $-1/2$ and $1/2$ corresponding to a random phase difference due to spatial incoherence. In the coherent case we get:

$$\begin{aligned} I(\mathbf{d}) &\propto |E_s(\mathbf{d}) + E_s(\mathbf{d}) \exp(\frac{2\pi i \Delta l}{\lambda})|^2 = \\ &= 2|E_s(\mathbf{d})|^2 + 2|E_s(\mathbf{d})|^2 \cos(2\pi \Delta l/\lambda) \end{aligned} \tag{4.19}$$

while in the incoherent case we have

$$\begin{aligned} E(\mathbf{d},X) &= E_s(\mathbf{d}) + E_s(\mathbf{d})\exp(2\pi iX) \\ I(\mathbf{d}) &\propto \int_{-1/2}^{1/2} |E(\mathbf{d},X)|^2 dX = 2|E_s(\mathbf{d})|^2 \end{aligned} \tag{4.20}$$

where $I(\mathbf{d})$ is the observed diffracted intensity. Notice that in the incoherent case the term $2|E_s(\mathbf{d})|^2\cos(2\pi\Delta l/\lambda)$, which gives information about the relative location of the two electrons, is not present. This term is usually called the cross term and is the only one that gives structural information. The other term is called the self term, and this only gives information about the building blocks of the system, the electrons in this case, but not how they are organized.

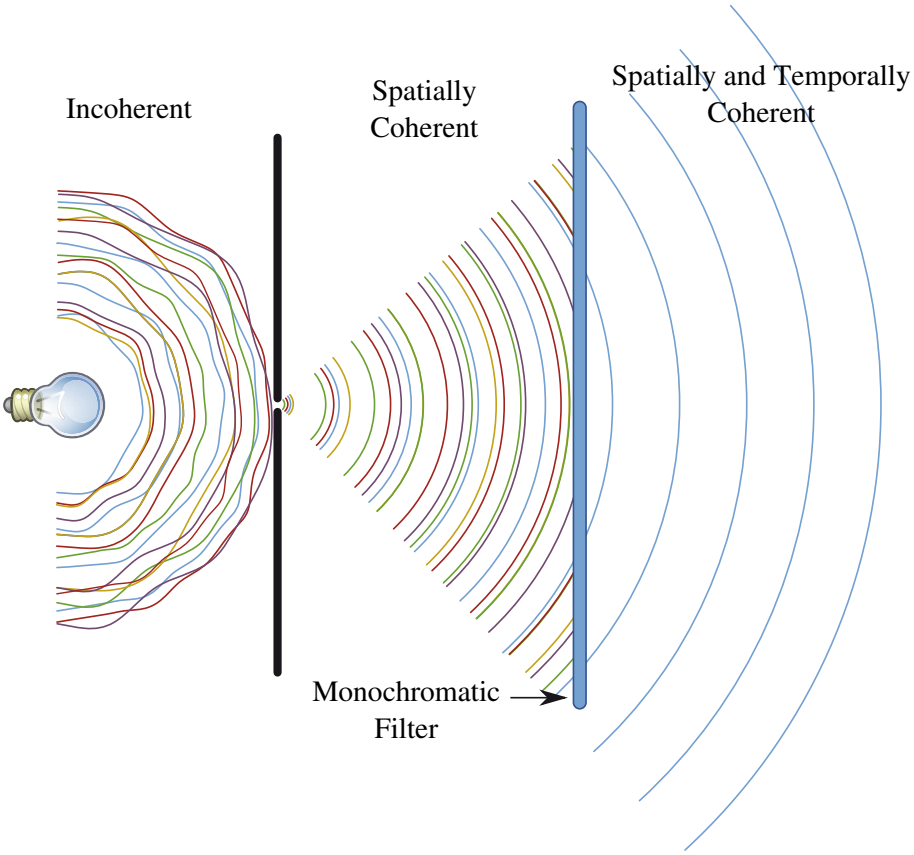

Figure 4.3: **Coherence.** A light bulb is a source of incoherent radiation, but by passing it through a pinhole it is possible to make it spatially coherent and by filtering it down to a single wavelength it is possible to make it temporally coherent.

Motion in the system during the exposure can also produce effects similar to the ones produced by an incoherent wave, if the motion is of the order of the

probing wavelength. In a way, one can say that the stability of the sample also affects the coherence of the diffraction experiment. This effect is analysed in detail in **paper IV**.

5. Image Reconstruction

In the previous chapter we have developed tools that allow us to predict and calculate the X-ray diffraction pattern from an arbitrary electron density, using mild assumptions, namely, that we are sufficiently far from the scatterer so that the Fraunhofer approximation holds, and that there is no multiple scattering. In this chapter we will try to tackle the *inverse problem*, that is, from an arbitrary diffraction pattern we will try to recover the electron density that gave rise to it. There are many special experimental conditions under which this problem can be solved relatively easily such as fourier holography [30, 13, 28], ptychography [36, 41], fresnel coherent diffractive imaging [34, 33], among others. In this chapter we will only deal with the general problem.

5.1 The Phase Problem

We have seen that a diffraction pattern can be calculated from the Fourier transform of the electron density. We have also seen in chapter 3 that the inverse of the Fourier transform is exactly like the Fourier transform, except with the sign of the exponent swapped. So we should be able to recover the electron density by,

$$\rho(\mathbf{r}) = \int_{\mathbf{r}} F(\mathbf{S}) \exp(-2\pi i \mathbf{r}\cdot\mathbf{S})\, d\mathbf{S}. \tag{5.1}$$

In general, $F(\mathbf{S})$ is a complex number and unfortunately it is not possible to measure $F(\mathbf{S})$, but only its absolute value, also known as its amplitude. The phase, called sometimes the argument of $F(\mathbf{S})$, is not known and so this problem is often called the *phase problem*. One could try to reconstruct the object assuming that the phases have an arbitrary value, say 0, and use the experimental amplitudes, the square root of the measured intensities, but this usually gives an uninterpretable picture. On the other hand, if the phases were known and the amplitudes unknown, then the resulting picture is still quite similar to the original, suggesting that the phases carry more structural information than the amplitudes (see Fig. 5.1).

If nothing about the object being imaged is known then the problem is undetermined. For a pattern with N pixels we have $2N$ unknowns (the real and imaginary part of the object) but only N constraints. But if we know that the

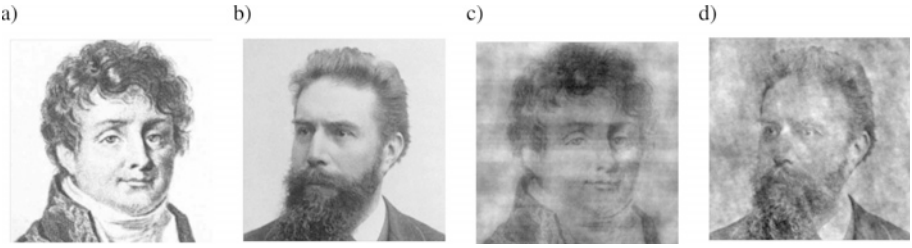

Figure 5.1: Portraits of Jean-Baptiste Fourier (a) and Wilhelm Röntgen (b). **c)** Fourier synthesis using the amplitudes from b and the phases from a. **d)** Fourier synthesis using the amplitudes from a and the phases from b.

object is isolated, meaning the object is surrounded by a constant ρ (e.g., sample in vacuum with a surrounding $\rho = 0$), then in some circumstances it is possible to solve this problem. The number of pixels of the object must at least be half of that of the diffraction pattern for the number of unknowns to match the number of constraints, that is, the oversampling ratio (see Fig. 3.3) of the image must be equal to or bigger than two, or equivalently the object must occupy less than half of the field of view. We will call images which fulfill this condition *oversampled*.

But this is not enough to solve the problem. In fact it has long been known that the problem is often undetermined in the one dimensional case [42]. Fortunately, for higher dimensions, it has been proven that most oversampled patterns have unique solutions [8]. This difference derives from the fact that one-dimensional polynomials are factorizable unlike two or higher dimensional ones.

5.2 Image Reconstruction Algorithms

Knowing that the two or higher dimensional phasing problem for oversampled patterns has a unique solution in most cases can serve as a starting point to solve the phase problem, but a method to find that unique solution is still necessary. The phase problem is remarkably difficult since it is neither a linear nor a convex problem. That makes it a nonconvex problem in a very high dimensional space, which is a class of problems that is very challenging.

In 1972 Gerchberg and Saxton [19] introduced an iterative algorithm to solve a related problem, that of obtaining phase information using both the diffraction pattern and an electron micrograph of a sample. The iteration starts by Fourier transforming the real space input, $\rho_i(\mathbf{x})$. The algorithm then replaces the resulting amplitudes with the square root of the intensities, $I(\mathbf{S})$. The result is then back Fourier transformed and the amplitudes of the resulting images are replaced by the ones from the electron micrograph $M(\mathbf{r})$.

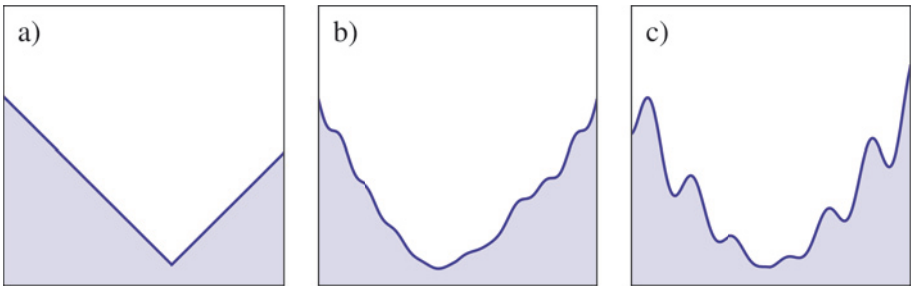

Figure 5.2: Function to be minimized for a linear (a), convex (b) and nonconvex (c) optimization problems.

Algorithm 5.1 Gerchberg-Saxton Iteration

$F_i(\mathbf{S}) \leftarrow \mathcal{F}\{\rho_i(\mathbf{r})\}$
$F_{i+1}(\mathbf{S}) \leftarrow \sqrt{I(\mathbf{S})}\frac{F_i(\mathbf{S})}{|F_i(\mathbf{S})|}$
$\rho_{i+1}(\mathbf{r}) \leftarrow M(\mathbf{r})\frac{\mathcal{F}^{-1}\{F_{i+1}(\mathbf{S})\}}{|\mathcal{F}^{-1}\{F_{i+1}(\mathbf{S})\}|}$

In 1978 Fienup [16], inspired by the above algorithm, introduced the error reduction algorithm to solve the phasing problem. Instead of using the electron micrograph as constraints in real space Fienup introduced the concept of a *support* function, $\Pi(\mathbf{r})$, which is equal to 1 where the object is allowed to reside and 0 otherwise. The iteration is analogous to the Gerchberg-Saxton Iteration but the last step is replaced by setting all points outside the support to 0.

Algorithm 5.2 Error Reduction Iteration

$F_i(\mathbf{S}) \leftarrow \mathcal{F}\{\rho_i(\mathbf{r})\}$
$F_{i+1}(\mathbf{S}) \leftarrow \sqrt{I(\mathbf{S})}\frac{F_i(\mathbf{S})}{|F_i(\mathbf{S})|}$
$\rho_{i+1}(\mathbf{r}) \leftarrow \Pi(\mathbf{r})\mathcal{F}^{-1}\{F_{i+1}(\mathbf{S})\}$

By applying this procedure iteratively it is possible to recover the correct solution. Unfortunately, more than often the algorithm gets stuck in local minima and cannot find the global minimum.

5.2.1 Iterations as Projections

In 1984 Levi and Stark realized that the above iterations can be interpreted as projections in Hilbert space [22]. This provides a particularly powerful method for trying to understand these algorithms. Let us call the replacement of the Fourier space amplitudes with the square root of the intensities the modulus projection, P_m, and the replacement of the image outside of the support

with 0, the support projection, P_s. If one treats the real space image as a vector in a high dimensional space, with one dimension per pixel, then it is easy to see that P_s is the projection into the hyperplane spanned by the dimensions corresponding to pixels inside the support. The modulus projection can also be interpreted as a projection in the space of the pixels of the diffraction pattern, where each pixel contributes two dimensions, the real part and the imaginary part (see Fig. 5.3).

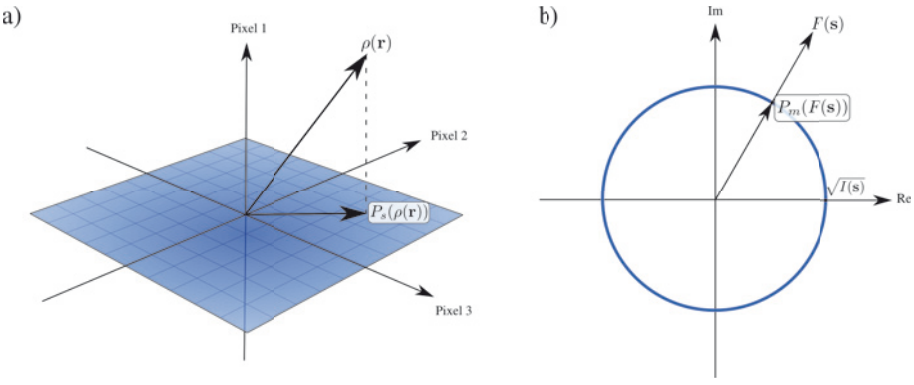

Figure 5.3: **a)** Support projection for a 3 pixel image where the support is composed of pixels 2 and 3. **b)** Modulus projection for 1 pixel of the diffraction pattern.

Due to the distance preserving property of the Fourier transform the modulus projection is also a projection in real space. The biggest difference between the two projection is that while the support constraint set is convex, the modulus constraint is not, that is to say, not all points between two points of the modulus constraint set belong to the modulus constraint set.

In this framework of projections the Error Reduction algorithm is simply the modulus projection (P_m) followed by the support projection (P_s). The fact that it stagnates can then be easily understood in connection to the non convexity of the modulus constraint as Fig. 5.4 illustrates.

In 1982 Fienup introduced the Hybrid Input-Output(HIO) algorithm [17] which is defined as:

Algorithm 5.3 Hybrid Input-Output Iteration

$$F_i(\mathbf{S}) \leftarrow \mathcal{F}\{\rho_i(\mathbf{r})\}$$
$$F_{i+1}(\mathbf{S}) \leftarrow \sqrt{I(\mathbf{S})}\frac{F_i(\mathbf{S})}{|F_i(\mathbf{S})|}$$
$$\rho'(\mathbf{r}) \leftarrow \mathcal{F}^{-1}\{F_{i+1}(\mathbf{S})\}$$
$$\rho_{i+1}(\mathbf{r}) \leftarrow \Pi(\mathbf{r})\rho'(\mathbf{r}) + (1-\Pi(\mathbf{r}))(\rho_i(\mathbf{r}) - \beta\rho'(\mathbf{r}))$$

which can also be represented with projection operators [40] as:

$$\rho_{i+1} = \rho_i + \beta\left[P_s((1+\beta^{-1})P_m(\rho_i) - \beta^{-1}\rho_i) - P_m(\rho_i)\right]. \qquad (5.2)$$

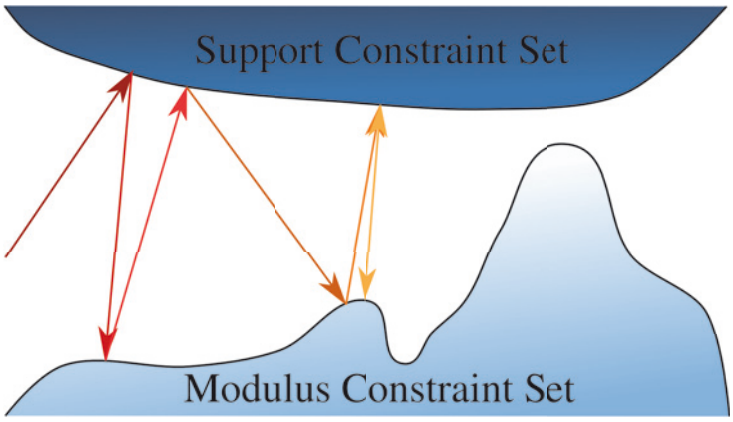

Figure 5.4: Successive iterations of the Error Reduction algorithm represented as interconnecting vectors of different shades of orange. The algorithm stagnates on a local minimum due to the non convexity of the modulus constraint set.

This means that the change in each iteration is a sum of a point projected onto the support constraint minus a point projected onto the modulus constraint all scaled by a relaxation factor β (see Fig. 5.5). If the separation between the two projections is large, the step length will be large and the algorithm will probably explore some other areas. This means that the algorithm is quite good at getting out of local minima, but also means that if the sets never get too close (due to noisy data for example), this algorithm will have a difficult time keeping close to the best solution, even though it might pass through it.

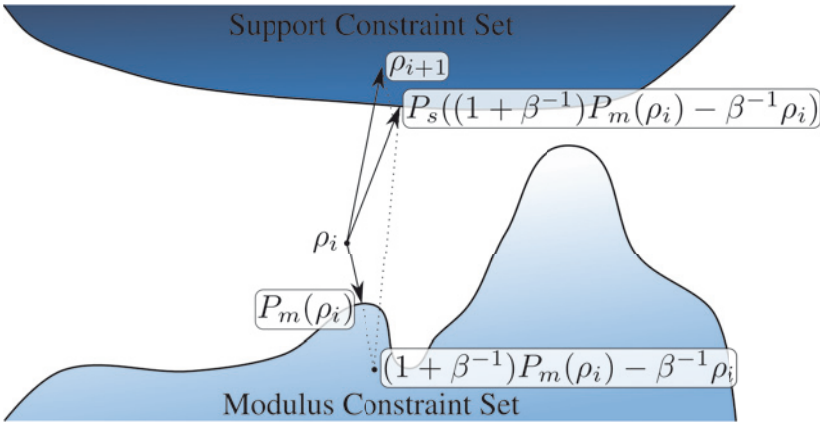

Figure 5.5: One iteration of the HIO algorithm assuming the origin is at ρ_i. Note that the iteration does not end at the surface of the constraint set.

The HIO algorithm was a tremendous improvement and it is still widely used today. It is probably the most popular algorithm for phase retrieval.

5.2.2 Shrinkwrap algorithm

While the HIO algorithm produces very good results when a tight support is known, for many applications it is hard to know in advance the shape of the support, and a support that is too large can make phasing impossible in practice.

In 2003 Marchesini [27] introduced the *Shrinkwrap algorithm* which does not require the support function as input and tries instead to deduce it during the reconstruction. It does so by starting with a support derived from the autocorrelation, where all pixels above a certain threshold are included in the support. It then refines the support every n iterations by blurring the current best guess of the object and keeping in the support only those pixels that are above a certain threshold of the maximum pixel value. The value of n is typically a couple dozen iterations. The idea of the algorithm is that even with a bad support some features of the objects will start to show up, so it makes use of those recovered features to improve the support. This algorithm has been remarkably successful in reconstructing several experimental data sets [10, 5, 4] and was also used for image reconstruction in **papers I,III and IV**.

5.3 Image reconstruction software

Even though there is a large number of algorithms and techniques published for image reconstruction from CXDI diffraction patterns, there is, to our knowledge, no publicly available software package that integrates all these tools into an easy to use package.

Hawk, is an open source software package for data processing, which is being developed in Uppsala, with the aim to fill this gap (**paper V**). It is publicly available under the GNU General Public License at `http://xray.bmc.uu.se/hawk` and implements the following phasing algorithms: HIO [17], RAAR [25], difference map [14], HPR [7], HAAR [6], ESPRESSO [26] and charge flipping [31, 32]. It is also capable to leverage graphic processing units, using the Compute Unified Device Architecture(CUDA) providing very large speedups, between 10x to 50x, compared to classic CPU based programs.

6. Perspectives

LCLS has just started user operations. A revamped FLASH will come back to life in August 2010. Fermi in Trieste will become operational in the autumn, and the European XFEL will be ready in 2014. In the meantime, table-top and pocket-sized instruments are popping up. These are very interesting times. The experimental verification that it is possible to obtain a high resolution image of a sample using ultrafast CXDI before the sample is turned into plasma (**Paper I**) opens the door to many exciting possibilities in the field of structural biology and nano imaging in general.

High resolution 2D CXDI pictures of unmodified large biological entities such as cells and organelles are already in our reach. The refinement of experimental conditions and the accumulated experience is likely to bring the resolution achieved in line with the radiation damage limit (**Paper VI**).

The possibility of obtaining high resolution 3D structures of reproducible objects such as virus or proteins is within our horizon. Still formidable problems have to be tackled, due to the extremely low signal to noise levels expected from the diffraction patterns of such small samples, even when using the spectacular brilliance of X-ray FELs. Another challenge is assembling several 2D diffraction patterns into a 3D diffraction volume when the orientation of the sample is unknown and the noise is large. But several papers have shown that the problem is tractable [15, 24, 18], all what is missing is an experimental demonstration. The computational cost of these approaches is extremely high so a strong investment in high performance parallel software allied with a similar investment in hardware will be crucial to bring these ideas to fruition. GPUs are expected to play an important role in this respect as they are progressing faster than CPUs and for most CXDI related algorithms they are much more efficient in terms of number of computations executed per energy used.

The potential for pump-probe experiments is also enormous and only now starting to be fully realized. Photo-activated reactions are particularly exciting in this regards, such as imaging photosynthesis as it happens.

The quality of the beam produced by the newly built X-ray FELs is also continuously improving leading to better resolution, both temporally and spatially.

We are at a start of a revolution when it comes to structural sciences. The future is most promising!

7. Sammanfattning på svenska

Mänskligheten har alltid haft en fascination för att kunna se oändligt små saker. Sedan uppfinningen av mikroskop har människor försökt att hitta sätt att titta på mindre och mindre saker. Optisk mikroskopi är otroligt bra men upplösningen är i grunden begränsad av våglängden för synligt ljus, vilken är runt 400nm för ultraviolett ljus.

Uppfinningen av röntgenkristallografi i början av nittonhundratalet gjorde det möjligt att observera strukturer mycket mindre än våglängden för synligt ljus. Vid kristallografi används vanligtvis ljus med en våglängd runt 1 Å, 4000 gånger mindre än violett ljus. Detta betyder att det är möjligt att observera saker som är 4000 gånger mindre.

Tyvärr har röntgenstrålning några nackdelar jämfört med synligt ljus, det viktigaste av allt är att dess brytningsindex alltid är mycket nära ett vilket innebär att det i praktiken är omöjligt att bygga konventionella linser. Därför finns det ingen exakt motsvarighet till optiska mikroskop. Istället för att avbilda föremålet direkt är det bästa vi kan göra att mäta diffraktionsmönster. Diffraktionsmönstrett skiljer sig helt från objektet självt, men under vissa förhållanden är det möjligt att rekonstruera bilden av objektet från dess diffraktionsmönster, detta kallas för fasning. Svårigheten med fasningen är att det inte är möjligt att direkt beräkna objektet som gav upphov till ett visst diffraktionsmönster. Istället måste man beräkna diffraktionsmönster från många objekt tills man hittar ett som passar det experimentella diffraktionsmönstret. Detta kan ses som att vi ersätter linsen i det optiska mikroskopet med en dator (se Figur. 7.1).

En annan svårighet med att avbilda mycket små strukturer är att de sprider ljuset mycket svagt. Inom Röntgenkristallografi löses detta problem genom användandet av kristaller som består av många små identiska objekt. Koherent avbildning med röntgendiffraktion (CXDI, från engelskans “Coherent X-ray Diffractive Imaging”) använder mycket intensiva ljuskällor, endast möjligt tack vare nyutvecklade röntgenlasrar, för att uppnå samma mål. Problemet med mycket intensiva ljuskällor är att de förstör vårt prov, på samma sätt som en stark laser kan bränna objekt. För att lösa detta problem använder CXDI en annan egenskap hos röntgenlasrar, det faktum att röntgenstrålarna produceras i extremt korta pulser. Detta gör det möjligt att få en bild av vårt prov precis innan det bränns upp av lasern.

Denna avhandling presenterar några av de första resultaten av CXDI med röntgenlasrar. Den undersöker också numeriskt några av de problem

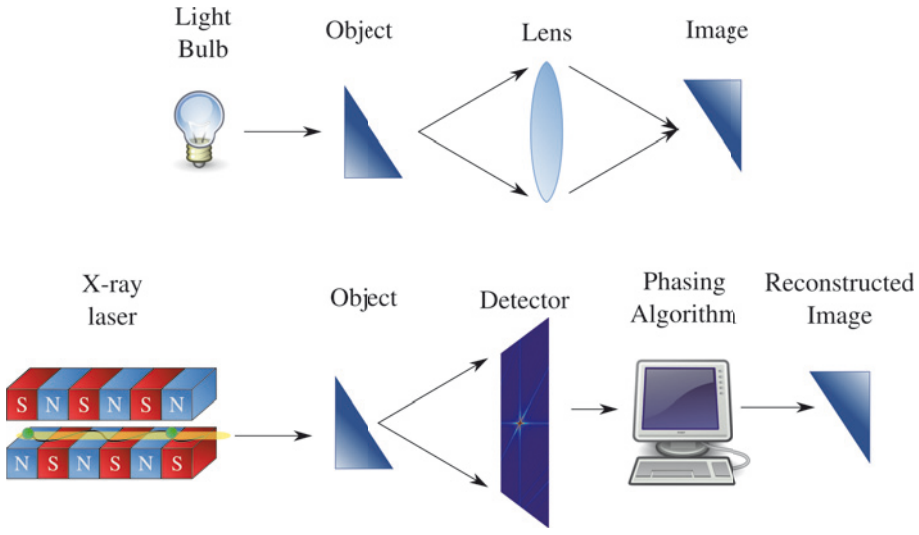

Figure 7.1: Jämförelse av avbildning med en lins och diffraktionsavbildning där linsen ersatts med en fasningsalgoritm i en dator.

som måste lösas för att denna teknik ska kunna bli lika vanlig som röntgenkristallografi.

Idag finns det relativt få bilder som erhållits genom CXDI eftersom de första röntgenlasrarna med tillräcklig prestanda nyligen färdigställts och många detaljer fortfarande optimeras. Allt pekar dock på en enorm ökning av användandet av tekniken och en stor förbättring av upplösningen. Vi står idag vid början av en revolution av vetenskapen om strukturbestämmning. Framtiden är mycket lovande!

Acknowledgements

These six years that I spent in Uppsala, first as an Erasmus student and then as a PhD student, were some of the best ones in my life. All the new things that I experienced and the different people that supported me during this time are the reason for it.

I would like to thank my supervisor, Janos, for first bringing me into the group during my exchange period and then offering me the opportunity to do this PhD, as well as always giving me the freedom to work in what I find interesting. Also many thanks to both Janos and Inger for several amazing sailing trips during some glorious summer weekends.

To my co-supervisor David I am very grateful for the constant support, including helping me write my first paper, inspiring discussions during lunch time which helped me solve problem after problem, as well as continuous encouragement to publish my ideas.

I would also like to thank:

Nic, for never being quiet and for all the assistance with my math difficulties.

Abraham and Hanna, for all the guidance, specially in the beginning, and for all the insightful conversations and new interesting ideas that you introduced me to.

Tomas, for always listening to all my silly questions, for countless hours of great discussions in front of the blackboard, even when the computers were working, and for being a fantastic office-mate.

Gösta, for introducing me to diffractive imaging, Ultimate Frisbee games and for a memorable trip to California.

Calle, for inspiring me to finish my PhD.

Michiel, Pavel, Pavel, Anne and Rafal for many hours of card playing and good fun.

Tiago, for an unforgettable first six months.

Elsa, Daniel, for giving me the opportunity to practise Portuguese.

Magnus, Alexandra, Sara, Johan, Erik, Marvin, Martin, Gunilla, Karin, Daniel, Bianca, Malin, Duško, Daniel, Jakob, Jochen, Olof for the fun company during fika and for making a terrific lab.

The great bunch of guys from Flogsta building 5 second floor during the fall of 2004, for keeping me up during a harsh winter.

All the exchange students in the Döbelnsgatan exchange student corridor between 2005 and 2007, for the warm company and happy parties.

To allihopa@xray, for creating a pleasant working environment.

To all the administrative personal at ICM, particularly Sigrid, for always taking care of any problems.

To everyone at the FLASH and LCLS beamtimes, for making them more enjoyable.

All my co-authors, it was a pleasure and an honour to work with you all.

My family for the immense support and encouragement you have given me throughout all these years.

To Aušra, for making me the happiest person in the world.

The author's contribution

Publications included in this thesis

Paper I:

H. Chapman et al. ***"Femtosecond diffractive imaging with a soft-X-ray free-electron laser"***
I was involved in the data analysis and image reconstruction.

Paper II:

D. van der Spoel et al. ***" Structural studies of melting on the picosecond time scale"***
I did all the X-ray diffraction calculations and large parts of the writing related to it.

Paper III:

A. Ravasio et al. ***" Single-Shot Diffractive Imaging with a Table-Top Femtosecond Soft X-Ray Laser-Harmonics Source"***
I did all the data analysis and image reconstructions and wrote the corresponding sections of the paper.

Paper IV:

F. R. N. C. Maia et al. ***"Structural variability and the incoherent addition of scattered intensities in single-particle diffraction"***
The idea was generated from my observations of previous reconstruction projects. I did all the diffraction simulations and image reconstruction as well as most of the analysis and writing of the paper.

Paper V:

F. R. N. C. Maia et al. ***"Hawk: the image reconstruction package for coherent X-ray diffractive imaging"***
I coded most of the software and wrote most of the paper.

Supporting publications

Paper VI:

M. Bergh et al. ***"Feasibility of imaging living cells at subnanometer resolutions by ultrafast X-ray diffraction"***
I contributed to the calculations and writing of section on depth information from diffraction experiments.

Paper VII:

M. J. Bogan et al. ***"Single particle X-ray diffractive imaging"***
I was involved in the preparation and implementation of the experiment at FLASH as well as data analysys and image reconstruction.

Bibliography

[1] W. Ackermann, G. Asova, V. Ayvazyan, A. Azima, N. Baboi, J. Bahr, V. Balandin, B. Beutner, A. Brandt, A. Bolzmann, R. Brinkmann, O. I. Brovko, M. Castellano, P. Castro, L. Catani, E. Chiadroni, S. Choroba, A. Cianchi, J. T. Costello, D. Cubaynes, J. Dardis, W. Decking, H. Delsim-Hashemi, A. Delserieys, G. Di Pirro, M. Dohlus, S. Dusterer, A. Eckhardt, H. T. Edwards, B. Faatz, J. Feldhaus, K. Flottmann, J. Frisch, L. Frohlich, T. Garvey, U. Gensch, Gerthch, M. Gorler, N. Golubeva, H. J. Grabosch, M. Grecki, O. Grimm, K. Hacker, U. Hahn, J. H. Han, K. Honkavaara, T. Hott, M. Huning, Y. Ivanisenko, E. Jaeschke, W. Jalmuzna, T. Jezynski, R. Kammering, V. Katalev, K. Kavanagh, E. T. Kennedy, S. Khodyachykh, K. Klose, V. Kocharyan, M. Korfer, M. Kollewe, W. Koprek, S. Korepanov, D. Kostin, M. Krassilnikov, G. Kube, M. Kuhlmann, C. L. S. Lewis, L. Lilje, T. Limberg, D. Lipka, F. Lohl, H. Luna, M. Luong, M. Martins, M. Meyer, P. Michelato, V. Miltchev, W. D. Moller, L. Monaco, W. F. O. Muller, O. Napieralski, O. Napoly, P. Nicolosi, D. Nolle, T. Nunez, A. Oppelt, C. Pagani, R. Paparella, N. Pchalek, J. Pedregosa-Gutierrez, B. Petersen, B. Petrosyan, G. Petrosyan, L. Petrosyan, J. Pfluger, E. Plonjes, L. Poletto, K. Pozniak, E. Prat, D. Proch, P. Pucyk, P. Radcliffe, H. Redlin, K. Rehlich, M. Richter, M. Roehrs, J. Roensch, R. Romaniuk, M. Ross, J. Rossbach, V. Rybnikov, M. Sachwitz, E. L. Saldin, W. Sandner, H. Schlarb, B. Schmidt, M. Schmitz, P. Schmuser, J. R. Schneider, E. A. Schneidmiller, S. Schnepp, S. Schreiber, M. Seidel, D. Sertore, A. V. Shabunov, C. Simon, S. Simrock, E. Sombrowski, A. A. Sorokin, P. Spanknebel, R. Spesyvtsev, L. Staykov, B. Steffen, F. Stephan, F. Stulle, H. Thom, K. Tiedtke, M. Tischer, S. Toleikis, R. Treusch, D. Trines, I. Tsakov, E. Vogel, T. Weiland, H. Weise, M. Wellhofer, M. Wendt, I. Will, A. Winter, K. Wittenburg, W. Wurth, P. Yeates, M. V. Yurkov, I. Zagorodnov, and K. Zapfe. Operation of a free-electron laser from the extreme ultraviolet to the water window. *Nature Photonics*, 1(6):336–342, June 2007.

[2] G. Adamo, K. F. MacDonald, Y. H. Fu, C. M. Wang, D. P. Tsai, F. J. Garc'ia de Abajo, and N. I. Zheludev. Light well: A tunable free-electron light source on a chip. *Physical Review Letters*, 103(11):113901+, Sep 2009.

[3] D. T. Attwood. *Soft X-rays and extreme ultraviolet radiation: principles and applications*. Cambridge University Press, The Edinburgh Building, Cambridge, CB2 2RU, UK, 2007.

[4] A. Barty, S. Marchesini, H. N. Chapman, C. Cui, M. R. Howells, D. A. Shapiro, A. M. Minor, J. C. Spence, U. Weierstall, J. Ilavsky, A. Noy, S. P. Hau-Riege, A. B. Artyukhin, T. Baumann, T. Willey, J. Stolken, T. van Buuren, and J. H.

Kinney. Three-dimensional coherent x-ray diffraction imaging of a ceramic nanofoam: determination of structural deformation mechanisms. *Physical review letters*, 101(5), August 2008.

[5] Anton Barty, Sebastien Boutet, Michael J. Bogan, Stefan Hau-Riege, Stefano Marchesini, Klaus Sokolowski-Tinten, Nikola Stojanovic, Ra'anan Tobey, Henri Ehrke, Andrea Cavalleri, Stefan Dusterer, Matthias Frank, Sasa Bajt, Bruce W. Woods, Marvin M. Seibert, Janos Hajdu, Rolf Treusch, and Henry N. Chapman. Ultrafast single-shot diffraction imaging of nanoscale dynamics. *Nature Photonics*, 2(7):415–419, June 2008.

[6] H. Bauschke, P. Combettes, and D. Luke. A strongly convergent reflection method for finding the projection onto the intersection of two closed convex sets in a hilbert space. *Journal of Approximation Theory*, 141(1):63–69, July 2006.

[7] H. H. Bauschke, P. L. Combettes, and D. R. Luke. Hybrid projection-reflection method for phase retrieval. *J Opt Soc Am A Opt Image Sci Vis*, 20(6):1025–1034, June 2003.

[8] Y. Bruck and L. Sodin. On the ambiguity of the image reconstruction problem. *Optics Communications*, 30(3):304–308, September 1979.

[9] Henry N. Chapman, Anton Barty, Michael J. Bogan, Sebastien Boutet, Matthias Frank, Stefan P. Hau-Riege, Stefano Marchesini, Bruce W. Woods, Sasa Bajt, Henry W. Benner, Richard A. London, Elke Plonjes, Marion Kuhlmann, Rolf Treusch, Stefan Dusterer, Thomas Tschentscher, Jochen R. Schneider, Eberhard Spiller, Thomas Moller, Christoph Bostedt, Matthias Hoener, David A. Shapiro, Keith O. Hodgson, David van der Spoel, Florian Burmeister, Magnus Bergh, Carl Caleman, Gosta Huldt, Marvin M. Seibert, Filipe R. Maia, Richard W. Lee, Abraham Szoke, Nicusor Timneanu, and Janos Hajdu. Femtosecond diffractive imaging with a soft-x-ray free-electron laser. *Nature Physics*, 2(12):839–843, November 2006.

[10] Henry N. Chapman, Anton Barty, Stefano Marchesini, Aleksandr Noy, Stefan P. Hau-Riege, Congwu Cui, Malcolm R. Howells, Rachel Rosen, Haifeng He, John C. Spence, Uwe Weierstall, Tobias Beetz, Chris Jacobsen, and David Shapiro. High-resolution ab initio three-dimensional x-ray diffraction microscopy. *Journal of the Optical Society of America A*, 23(5):1179–1200, May 2006.

[11] Henry N. Chapman, Stefan P. Hau-Riege, Michael J. Bogan, Sasa Bajt, Anton Barty, Sebastien Boutet, Stefano Marchesini, Matthias Frank, Bruce W. Woods, Henry W. Benner, Richard A. London, Urs Rohner, Abraham Szoke, Eberhard Spiller, Thomas Moller, Christoph Bostedt, David A. Shapiro, Marion Kuhlmann, Rolf Treusch, Elke Plonjes, Florian Burmeister, Magnus Bergh, Carl Caleman, Gosta Huldt, Marvin M. Seibert, and Janos Hajdu. Femtosecond time-delay x-ray holography. *Nature*, 448(7154):676–679, August 2007.

[12] P. B. Corkum. Plasma perspective on strong field multiphoton ionization. *Physical Review Letters*, 71(13):1994–1997, Sep 1993.

[13] S. Eisebitt, J. Luning, W. F. Schlotter, M. Lorgen, O. Hellwig, W. Eberhardt, and J. Stohr. Lensless imaging of magnetic nanostructures by x-ray spectroholography. *Nature*, 432(7019):885–888, December 2004.

[14] Veit Elser. Phase retrieval by iterated projections. *Journal of the Optical Society of America A: Optics, Image Science, and Vision*, 20(1):40–55, 2003.

[15] Veit Elser. Noise limits on reconstructing diffraction signals from random tomographs. *IEEE Trans. Inf. Theor.*, 55(10):4715–4722, 2009.

[16] J. R. Fienup. Reconstruction of an object from the modulus of its fourier transform. *Opt. Lett.*, 3(1):27+, July 1978.

[17] J. R. Fienup. Phase retrieval algorithms: a comparison. *Applied Optics*, 21(15):2758–2769, 1982.

[18] Russell Fung, Valentin Shneerson, Dilano K. Saldin, and Abbas Ourmazd. Structure from fleeting illumination of faint spinning objects in flight. *Nature Physics*, 5(1):64–67, November 2008.

[19] R. W. Gerchberg and W. O. Saxton. A practical algorithm for the determination of the phase from image and diffraction plane pictures. *Optik*, 35:237–246, 1972.

[20] Stefan P. Hau-Riege. Effect of the coherence properties of self-amplified-spontaneous-emissionx-ray free electron lasers on single-particle diffractive imaging. *Opt. Express*, 16(4):2840–2844, February 2008.

[21] M. R. Howells, T. Beetz, H. N. Chapman, C. Cui, J. M. Holton, C. J. Jacobsen, J. Kirz, E. Lima, S. Marchesini, and H. Miao. An assessment of the resolution limitation due to radiation-damage in x-ray diffraction microscopy. *Journal of Electron Spectroscopy and Related Phenomena*, 170(1-3):4–12, March 2009.

[22] Aharon Levi and Henry Stark. Image restoration by the method of generalized projections with application to restoration from magnitude. *J. Opt. Soc. Am. A*, 1(9):932–943, September 1984.

[23] M. Lewenstein, Ph, Yu, Anne L'Huillier, and P. B. Corkum. Theory of high-harmonic generation by low-frequency laser fields. *Physical Review A*, 49(3):2117–2132, Mar 1994.

[24] Ne Te Duane Loh and Veit Elser. Reconstruction algorithm for single-particle diffraction imaging experiments. *Physical Review E (Statistical, Nonlinear, and Soft Matter Physics)*, 80(2):026705+, 2009.

[25] D. Russell Luke. Relaxed averaged alternating reflections for diffraction imaging. *Inverse Problems*, 21(1):37–50, 2005.

[26] S. Marchesini. Ab initio compressive phase retrieval. *arXiv:0809.2006v1 [physics.optics]*, Sep 2008.

[27] S. Marchesini, H. He, H. N. Chapman, Hau S. P. Riege, A. Noy, M. R. Howells, U. Weierstall, and J. C. H. Spence. X-ray image reconstruction from a diffraction pattern alone. *Physical Review B*, 68(14):140101, Oct 2003.

[28] Stefano Marchesini, Sebastien Boutet, Anne E. Sakdinawat, Michael J. Bogan, Sasa Bajt, Anton Barty, Henry N. Chapman, Matthias Frank, Stefan P. Hau-Riege, Abraham Szoke, Congwu Cui, David A. Shapiro, Malcolm R. Howells, John C. Spence, Joshua W. Shaevitz, Joanna Y. Lee, Janos Hajdu, and Marvin M. Seibert. Massively parallel x-ray holography. *Nature Photonics*, 2(9):560–563, August 2008.

[29] G. Materlik and T. Tschentscher. *TESLA Technical Design Report*. DESY, Hamburg, Germany, March 2001.

[30] Ian McNulty, Janos Kirz, Chris Jacobsen, Erik H. Anderson, Malcolm R. Howells, and Dieter P. Kern. High-resolution imaging by fourier transform x-ray holography. *Science*, 256(5059):1009–1012, May 1992.

[31] Gabor Oszlanyi and Andras Suto. Ab initio structure solution by charge flipping. *Acta Crystallographica Section A*, 60(2):134–141, 2004.

[32] Gábor Oszlányi and András Süto. *Ab initio* structure solution by charge flipping. II. Use of weak reflections. *Acta Crystallographica Section A*, 61(1):147–152, Jan 2005.

[33] H. M. Quiney, K. A. Nugent, and A. G. Peele. Iterative image reconstruction algorithms using wave-front intensity and phase variation. *Opt. Lett.*, 30(13):1638–1640, July 2005.

[34] H. M. Quiney, A. G. Peele, Z. Cai, D. Paterson, and K. A. Nugent. Diffractive imaging of highly focused x-ray fields. *Nature Physics*, 2(2):101–104, January 2006.

[35] A. Ravasio, D. Gauthier, F. R. N. C. Maia, M. Billon, J. P. Caumes, D. Garzella, M. Géléoc, O. Gobert, J. F. Hergott, A. M. Pena, H. Perez, B. Carré, E. Bourhis, J. Gierak, A. Madouri, D. Mailly, B. Schiedt, M. Fajardo, J. Gautier, P. Zeitoun, P. H. Bucksbaum, J. Hajdu, and H. Merdji. Single-shot diffractive imaging with a table-top femtosecond soft x-ray laser-harmonics source. *Physical Review Letters*, 103(2):028104+, Jul 2009.

[36] J. Rodenburg, A. Hurst, and A. Cullis. Transmission microscopy without lenses for objects of unlimited size. *Ultramicroscopy*, 107(2-3):227–231, February 2007.

[37] M. G. Rossmann and E. Arnold, editors. *International Tables for Crystallography*, volume F. Kluwer Academic Publishers, Dordrecht/Boston/London, first edition, 2001.

[38] C. E. Shannon. Communication in the presence of noise. *Proceedings of the IRE*, 37(1):10–21, January 1949.

[39] S. J. Smith and E. M. Purcell. Visible light from localized surface charges moving across a grating. *Physical Review Online Archive (Prola)*, 92(4):1069+, Nov 1953.

[40] P. Thibault. *Algorithmic methods in diffraction microscopy*. PhD thesis, Cornell University, August 2007.

[41] Pierre Thibault, Martin Dierolf, Oliver Bunk, Andreas Menzel, and Franz Pfeiffer. Probe retrieval in ptychographic coherent diffractive imaging. *Ultramicroscopy*, 109(4):338–343, March 2009.

[42] Adriaan Walther. The question of phase retrieval in optics. *Optica Acta: International Journal of Optics*, 10(1):41–49, 1963.

[43] L. W. Whitehead, G. J. Williams, H. M. Quiney, D. J. Vine, R. A. Dilanian, S. Flewett, K. A. Nugent, A. G. Peele, E. Balaur, and I. McNulty. Diffractive imaging using partially coherent x rays. *Physical Review Letters*, 103(24):243902+, Dec 2009.

Acta Universitatis Upsaliensis

Digital Comprehensive Summaries of Uppsala Dissertations from the Faculty of Science and Technology 731

Editor: The Dean of the Faculty of Science and Technology

A doctoral dissertation from the Faculty of Science and Technology, Uppsala University, is usually a summary of a number of papers. A few copies of the complete dissertation are kept at major Swedish research libraries, while the summary alone is distributed internationally through the series Digital Comprehensive Summaries of Uppsala Dissertations from the Faculty of Science and Technology. (Prior to January, 2005, the series was published under the title "Comprehensive Summaries of Uppsala Dissertations from the Faculty of Science and Technology".)

Distribution: publications.uu.se
urn:nbn:se:uu:diva-121930

ACTA
UNIVERSITATIS
UPSALIENSIS
UPPSALA
2010